Visualization of vitamin A metabolism

Koenders, S.T.A.

Chapter 9

Summary and Future Prospects

General Summary

Aldehyde dehydrogenases (ALDHs) convert endogenous and exogenous reactive aldehydes into carboxylic acids to reduce or prevent cellular damage (see **Chapter 1**).[1–3] In addition, ALDHs perform an essential metabolic role in several cellular processes.[4–7] For example, retinoic acid is an important signaling lipid, generated by ALDHs. Retinoic acid controls many cellular and physiological functions via gene transcription.[8–13] Retinoic acid is produced by retinaldehyde dehydrogenases ALDH1A1, ALDH1A2 and ALDH1A3 from its precursor retinal.[14] Retinaldehyde dehydrogenases are tightly regulated via an inducible cellular expression pattern and by post-translation modifications.[15,16]

Current methods allow researchers to measure expression levels of these enzymes or general ALDH activity in cells or tissue, but not the activity of individual enzymes. New strategies are highly desired to visualize and quantify ALDH activity of specific enzymes in health and disease. The aim of this thesis was, therefore, to develop and apply new chemical tools to study the activity of ALDHs in complex biological samples.

In **Chapter 2**, the recent developments in the field of chemical probes to study lipid biology, especially in immunology, are summarized and potential avenues for future research are indicated.[17] Lipids perform numerous functions inside the cell, ranging from structural building block of membranes and energy storage to cell signaling. The mode of action of many signaling lipids has remained elusive due to their low abundance, high lipophilicity, and inherent instability. Various chemical biology approaches, such as photoaffinity or activity-based protein profiling methods, have recently been developed to shed light on the biological role of lipids, lipid-protein interactions and lipid processing enzymes.

For example, activity-based protein profiling (ABPP) is a powerful methodology to map enzyme activities in complex biological samples.[18,19] ABPP relies on activity-based probes containing an electrophilic warhead, which reacts with a conserved catalytic amino acid residue of an enzyme. Visualization of the probe targets via reporter groups, such as fluorophores or biotin, is performed by in-gel fluorescent scanning or chemical proteomics. Comparative and competitive ABPP are the two main applications used in this thesis. In comparative ABPP the abundance of active enzymes derived from different biological samples are studied, whereas competitive ABPP is used to determine the selectivity profile of an inhibitor.

Activity-based protein profiling of retinaldehyde dehydrogenases

Chapter 3 describes the design and synthesis of a first-in-class probe for ALDHs. Guided by the co-crystal structure of ALDH1A1, retinal was functionalized with an alkyne ligation handle and an electrophilic warhead. This led to the design of **LEI-945**.[20] A convergent synthesis route utilizing a key Wittig reaction was developed to synthesize **LEI-945**. This retinal-based probe was biologically validated in **Chapter 4**.

LEI-945 labelled ALDH1A1, ALDH1A2 and ALDH1A3 by a covalent interaction with their catalytic cysteines. In addition, the probe was able to detect endogenously expressed ALDHs in A549 lung cancer cells, including ALDH2, ALDH3A2 and ALDH3B1. **LEI-945** also revealed the selectivity profile of pan-ALDH inhibitor 4-diethylaminobenzaldehyde (DEAB) and retinal using competitive ABPP in A549 cells.

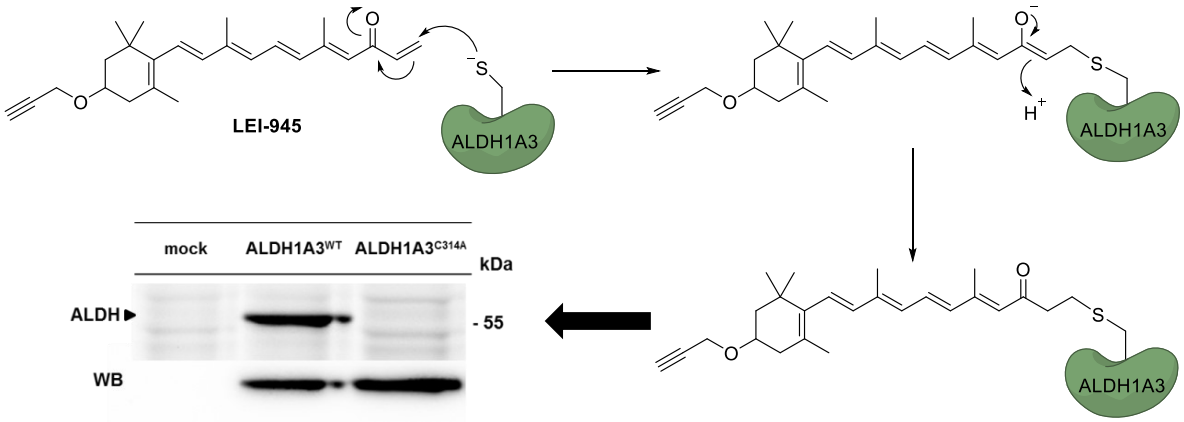

Fig. 9.1 | Covalent interaction of LEI-945 with and visualization of ALDH1A3. The vinyl ketone warhead of **LEI-945** undergoes nucleophilic attack by the catalytic cysteine of ALDH1A3. The resulting thioether cannot by hydrolyzed and results in an irreversible covalent interaction between ALDH1A3 and **LEI-945**. Ligation with AlexaFluor-647 and visualization by in-gel fluorescence showed a clear band around 55 kDa. Altering the catalytic cysteine into an alanine completely abolished labeling.

Profiling of ALDHs in breast cancer subtypes

Having established that **LEI-945** can act as an ABP for ALDHs, the probe was applied in **Chapter 5** for comparative ABPP using different breast cancer cell types. Upregulation of certain ALDHs has been previously linked to therapy resistance in cancer.[21] For example, ALDH1A3 is associated with poor clinical outcome in breast cancer.[22–26] The ALDEFLUOR assay, which is routinely used to measure ALDH activity, was not capable of predicting the ability of breast cancer cell lines to produce retinoic acid. Using **LEI-945** distinct ALDH activity profiles were made for each cell line. These profiles were used to explain the differences in retinal conversion based on the abundance of active ALDH1A1 and/or ALDH1A3 enzymes.

Remarkably, SK-BR-3, the breast cancer cell line showed the highest level of overall ALDH activity and displayed exceptionally high levels of active ALDH2, but converted a relatively low fraction of retinal. The low levels of ALDH1A3 activity in this cell line as determined by ABPP using **LEI-945** were sufficient to explain the conversion of retinal into retinoid acid. This suggested that human ALDH2 does not have a biologically relevant role in vitamin A metabolism.

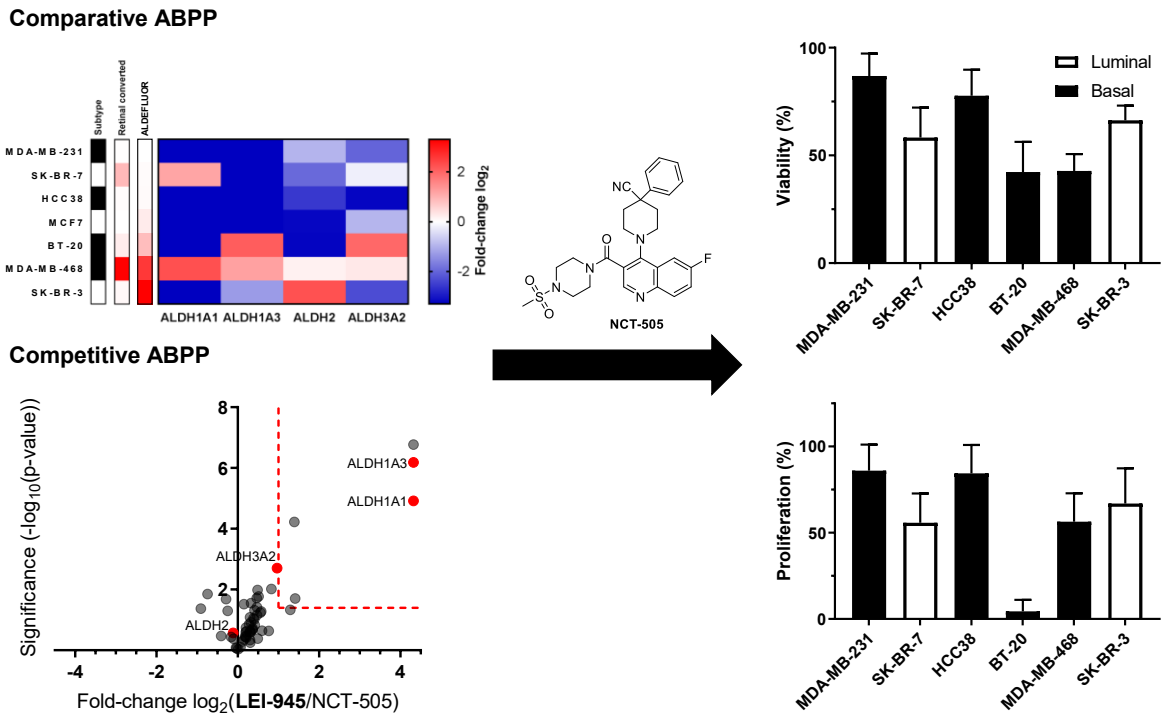

Fig. 9.2 | Comparative and competitive ABPP of ALDHs and subsequent cellular assays with NCT-505 in breast cancer cells. *Comparative ABPP:* ALDH profiling of breast cancer cell lines using chemical proteomics. The subtype column indicates if the cell line belongs to the luminal subtype (white) or basal subtype (black). The retinal converted column shows the amount of retinal converted to retinoic acid over 4 h in a gradient from 0% (white) to 100% (red). The ALDEFLUOR column shows the ALDH activity as determined by the ALDEFLUOR assay in a gradient from low (white) to high (red). The heatmap shows the fold-change in LFQ value for each ALDH enzyme compared to the average for each ALDH enzyme. $N = 2$ independent experiments with each at least $n = 3$ experiments per group (biological replicates). *Competitive ABPP:* Volcano plot of the *in situ* competitive ABPP experiment in MDA-MB-468 to determine off-targets of ALDH inhibitor NCT-505 (30 µM). $N = 4$ experiments per group (biological replicates). *Cellular assays:* cell viability of breast cancer cell lines after treatment with NCT-505 (30 µM) for 72 h. For viability and proliferation assay data represent mean values ± SD; $N = 3$ biological replicates with each $n = 3$ experiments per group.

LEI-945 was used for competitive ABPP in the MDA-MB-468 cell line to determine the selectivity profile of NCT-505, an advanced ALDH1A1 selective inhibitor.[27] Chemical proteomics analysis showed that NCT-505 inhibited both ALDH1A1 and ALDH1A3 and showcased the potential utility of **LEI-945** to guide drug discovery efforts toward selective ALDH inhibitors.

Combining the results from the comparative and competitive ABPP experiments, indicated that treatment of the breast cancer cell lines with the dual ALDH1A1/ALDH1A3 inhibitor would mostly affect the viability and proliferation of the SK-BR-7, BT-20 and MDA-MB-468 cell lines due to their high levels of ALDH1A1 or ALDH1A3 activity (**Fig. 9.2**). A slight decrease could also be detected for the SK-BR-3 cell line, which might be related to the relatively low amount of ALDH1A3 detected in these cells. Of note, the ALDEFLUOR assay did not show any ALDH activity in the SK-BR-7 cell line. This highlights the sensitivity of **LEI-945** to detect low amounts of ALDH activity, which might be used to guide the selection of (therapeutic) effective inhibitors.

Another way in which **LEI-945** could be applied in this field, is to study whether the reported increase in ALDH expression in 3D cell culture compared with 2D cell culture is accompanied by an increase in the activity levels of specific ALDH isozymes.[28,29] **LEI-945** could also be used in combination with the ALDEFLUOR assay and fluorescence-activated cell sorting, which is generally used to detect and sort therapy-resistant cancer (stem) cells. The sorted cell populations can be subjected to comparative ABPP, providing a better understanding of the underlying biology.[30] Although the research in this thesis has focused on the role of ALDH isozymes in breast cancer, it is envisioned that **LEI-945** could also be used to study the specific ALDH isozymes involved in other cancer types that express ALDHs.[25]

The role of ALDHs in lipid peroxidation

The physiological effects of ALDH1A1 and ALDH1A3 inhibition were studied in more depth by determining cellular ATP levels and using live cell imaging techniques. NCT-505 reduced ATP levels and the mitochondrial membrane potential. Analyzing cell states using FUCCI showed arrest of these cells in the G_1 phase of the cell cycle. A significant increase of propidium iodide staining indicated that the cells died via a necrosis-like pathway. Combination of NCT-505 with the glutathione peroxidase 4 (GPX4) inhibitor RSL3 had a therapeutically synergetic effect. RSL3 induces ferroptosis, which is an iron-dependent form of non-apoptotic cell-death.[31,32] Polyunsaturated fatty acids (PUFAs) can be oxidized by lipoxygenases into hydroxyperoxides.[33] Under normal conditions these reactive species are converted by GPX4 into lipid alcohols (**Fig. 9.3**).

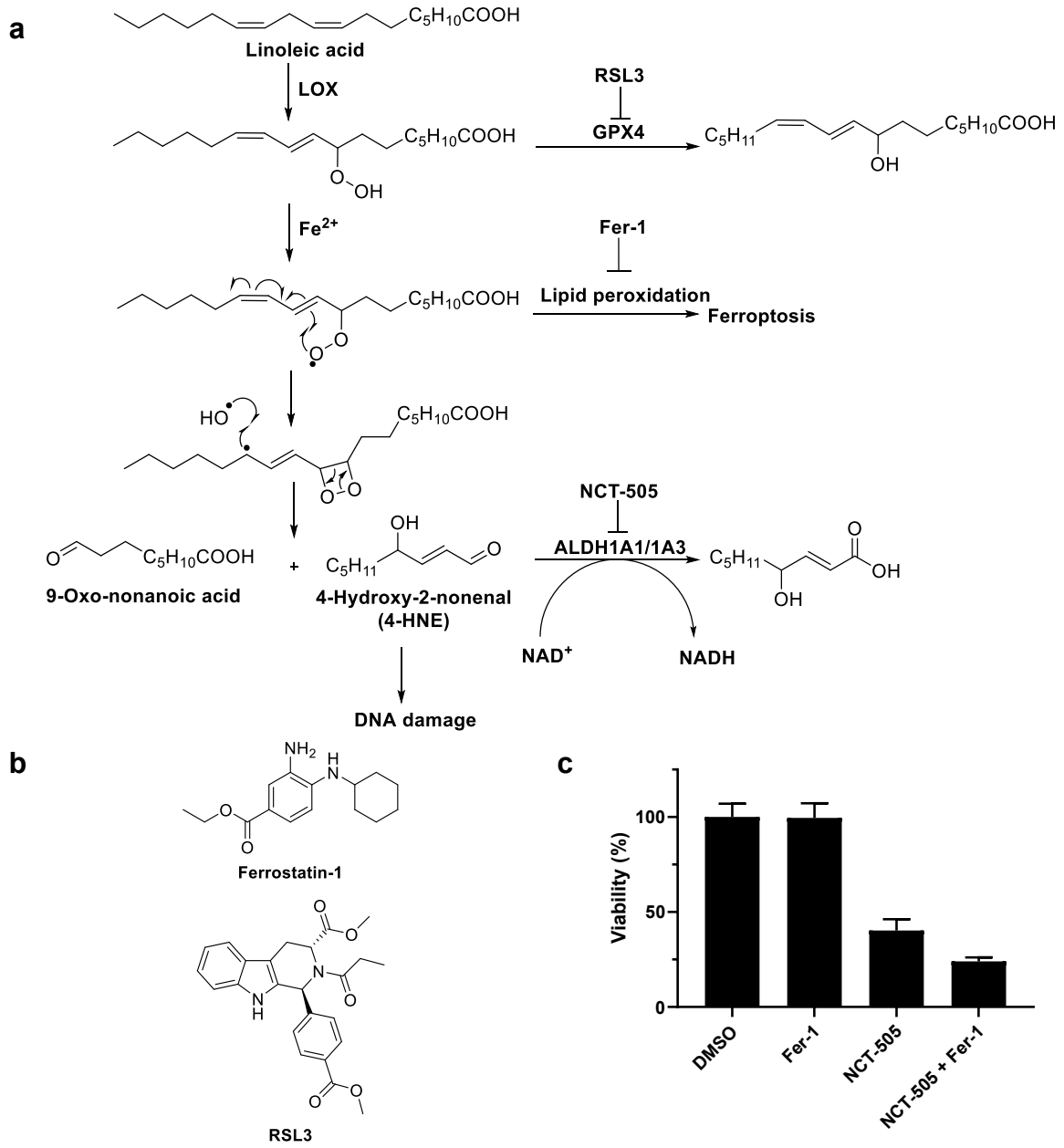

Fig. 9.3 | Overview of ferroptosis and lipid peroxidation. a, Schematic overview of ferroptosis and lipid peroxidation processes. Polyunsaturated fatty acid (PUFA), linoleic acid, is converted into a hydroperoxide by lipoxygenase (LOX). This hydroperoxide can then either be converted into a lipid alcohol by glutathione peroxidase 4 (GPX4) or a lipid radical under influence of iron. An accumulation of these lipid radicals induces ferroptosis, but this process can be inhibited by Fer-1. An alternative pathway is the formation of reactive aldehydes, such as 4-hydroxy-2-nonenal (4-HNE), which can bind to DNA. These reactive aldehydes are detoxified by aldehyde dehydrogenases (ALDHs) accompanied by the formation of NADH. ALDH1A1 and ALDH1A3 can be inhibited by NCT-505. **b**, Chemical structures of the radical trapping agent Ferrostatin-1 (Fer-1) and the GPX4 inhibitor RSL3. **c**, Graph showing the cell viability of MDA-MB-468 cells treated with DMSO, Fer-1 (10 μM), NCT-505 (30 μM) or Fer-1 (10 μM) and NCT-505 (30 μM). Data represent mean values ± SD; $n = 6$.

Inhibition of GPX4 by RSL3 results in an increase of lipid reactive oxygen species (ROS).[34] The propagation of these lipid radicals is catalyzed by iron and induces ferroptosis. Ferrostatin-1 (Fer-1; **Fig. 9.3b**), a radical trapping agent capable of blocking lipid radical propagation, was unable to rescue cells treated with NCT-505 and combinatorial treatment led to a significant (p = 0.0002) decrease in viability (**Fig. 9.3c**), suggesting that NCT-505 does not induce ferroptosis.

Effects of NCT-505 on MDA-MB-231 cells

Another interesting observation was made in NCT-505-treated MDA-MB-231 cells, which are derived from a triple-negative breast tumor. NCT-505 reduced the viability of the MDA-MB-231 cells to a small extent (**Fig. 9.2**), but it did induce a specific phenotype.

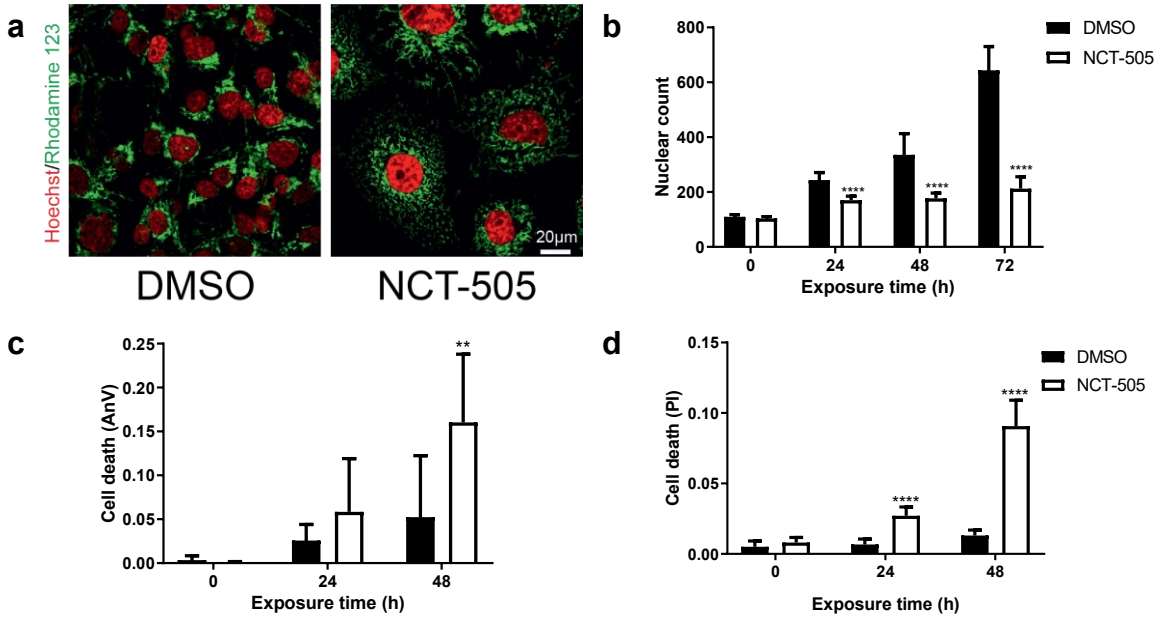

Fig. 9.4 | Effects of NCT-505 on MDA-MB-231 breast cancer cells. a, Representative images of live-cell confocal microscopy of mitochondrial potential after 72 h treatment with vehicle or NCT-505 (30 µM). Mitochondrial membrane potential was visualized using rhodamine 123 dye (green) while the nuclei were detected with Hoechst 33342 (red). **b**, Nuclear count of vehicle and NCT-505 (30 µM)-treated MDA-MB-231 cells measured over time. Data represent mean values ± SD; *N* = 3 biological replicates with each 3 experiments per group. **c**, Cell death profile of vehicle and NCT-505 (30 µM)-treated MDA-MB-231 cells as determined by Annexin V (AnV) staining and measured over time. **d**, Cell death profile of vehicle and NCT-505 (30 µM)-treated MDA-MB-231 cells as determined by propidium iodide (PI) staining and measured over time. For parts **c** and **d**, data represent mean values ± SD; *N* = 3 biological replicates with each 5 experiments per group. **P < 0.01 and ****P < 0.0001; *t* test, two-sided.

The volume of the cells was increased along with an expansion of the nucleus (**Fig. 9.4a**). This was accompanied with a decrease in cell motility (data not shown). This phenotype seems to resemble a senescent state. Further experimentation using specific biomarkers is required to confirm this hypothesis.[35]

Since, virtually no ALDH isozyme activity was detected in this cell line (**Fig. 9.2**), the observed phenotype is probably due to an off-target of NCT-505. Proteomics based methods, such as the cellular thermal shift assay (CETSA), can be applied to identify the target.[36,37] Another option would be to synthesize a probe based on the scaffold of NCT-505, which includes a photo-reactive cross-linker, such as a diazirine, for affinity-based protein profiling (A_fBPP).

Of note, cell imaging showed that the nuclear count of vehicle-treated cells increased more than 3-fold after 72 hours, whereas the nuclear count of NCT-505-treated MDA-MB-231 cells increased only marginally (**Fig. 9.4b**). This inhibition of cell proliferation was not detected in the Sulforhodamine B assay, which measures total protein content. These results highlight a benefit of live cell imaging.

Visualizing the role of vitamin A metabolism in immune homeostasis

Chapter 6 describes the search for the specific retinaldehyde dehydrogenases responsible for the conversion of retinal into retinoic acid in the small intestines of mice. Retinoic acid plays an important role in immune homeostasis via the activation and recruitment of dendritic, T and B cells.[38,39] Comparative ABPP of intestinal cells derived from *Aldh1a1*^{WT} and *Aldh1a1*$^{-/-}$ mice with **LEI-945** was performed and identified ALDH1B1 as a possible additional source of retinoic acid in intestinal epithelial cells.

Aldh1a1$^{-/-}$/*Aldh1b1*$^{-/-}$ mice showed a more proinflammatory phenotype, indicating involvement of both ALDH1A1 and ALDH1B1 in immune homeostasis. However, to determine whether the retinoid levels in the tissue of the small intestines from the knockout mice have actually changed, these levels will have to be quantified using liquid chromatography-mass spectrometry (LC-MS). The ability of *Aldh1a1*$^{-/-}$/*Aldh1b1*$^{-/-}$ intestinal epithelial cells to convert retinal into retinoic acid has not been assessed, but could be measured using the LC-UV/MS assay developed in **Chapter 4**.

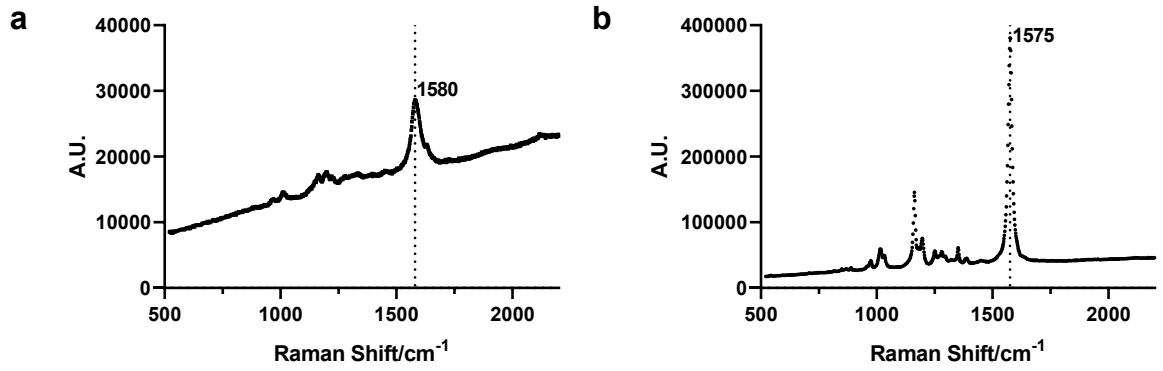

Fig. 9.5 | Raman spectra of clickable retinoids. a, Raman spectrum of **STA-211**. **b,** Raman spectrum of **STA-215**. For parts **a** and **b**, **s**pectra were acquired using 532 nm excitation, ca. 0.15 mW laser power, 20 s acquisition time and a spectral range of 500 to 2200 cm^{-1}. Characteristic peaks were identified at 1580 cm^{-1} and 1575 cm^{-1} for **STA-211** and **STA-215**, respectively.

Other sources of retinoic acid should also be considered, such as bile retinoids excreted from the liver in the form of retinoyl glucuronides[40,41] or the conversion of retinal into retinoic acid by the gut microbiome. ABPP of the gut microbiome using **LEI-945** could be used to identify bacterial enzymes and bacteria populations capable of this transformation.[42]

New chemical tools to study vitamin A interacting proteins are introduced in **Chapter 7**. These clickable vitamins were shown to be biologically equivalent to their endogenous counterparts and were applied for A_fBPP without the introduction of a photo-reactive group. Another envisioned application of these probes is to study the trafficking of retinoids between cells. One interesting new technique in this field is the application of Raman microscopy to track alkyne functionalized lipids in living cells.[43] This methods utilizes the characteristic peak of the alkyne at 2110 cm^{-1} in the biologically silent region of the Raman spectrum.[44] To determine the suitability of the clickable retinoids for this application, Raman spectra were acquired using 532 nm excitation, ca. 0.15 mW laser power and 20 seconds acquisition time in a spectral range from 500 to 2200 cm^{-1} (**Fig. 9.5a,b**).

The characteristic alkyne peak was not visible at these settings (which were 10-fold lower compared to similar experiments), but characteristic retinoid peaks of 1580 cm^{-1} and 1575 cm^{-1} were detected for the **STA-211** and **STA-215** probe, respectively.[45] The intrinsic characteristic signal of the retinoids is relatively intense and might be used to track retinoic exchange between cells depending on its signal-to-noise ratio.

Drug screening against aldehyde dehydrogenases using competitive ABPP

The development of an additional activity-based probe, **STA-55**, for aldehyde dehydrogenases is described in **Chapter 8**. This probe, derived from the reported ALDH inhibitor Aldi-2[46], was characterized as a broadspectrum probe for the ALDH family improving the coverage of the ALDH family by enriching ALDH1B1 and ALDH3A1 in addition to the ALDHs already enriched by **LEI-945** in A549 cells. It was subsequently used to determine the selectivity profile of three ALDH inhibitors by competitive ABPP.

This led to the discovery of another off-target of the ALDH1A1 inhibitor NCT-505[27] and revealed broadspectrum off-target activity for ALDH3A1 inhibitor CB7.[47] As **STA-55** enriched ALDH1A1 and ALDH3A1, both markers of cyclophosphamide resistance in cancer[48], it can potentially be used to predict therapy efficacy by identifying the activity of these enzymes in patient material. It may also be used in the development of new ALDH inhibitors by determining *in situ* target engagement and selectivity.

To determine whether **STA-55** truly covers the entire ALDH family the 13 remaining ALDH enzymes will have to be transiently overexpressed and subjected to labelling experiments. To enable efficient screening of selectivity profiles using ABPP, a cell line containing preferably all or at least the most clinically relevant ALDHs would be required. Thus far, the breast cancer MDA-MB-468 cell line has been used for screening, as it expresses both ALDH1A1 and ALDH1A3. Another candidate would be the lung cancer cell line A549, which proliferates rapidly and can be easily transfected.

Closing remarks

Several new chemical tools are presented in this thesis that enable the study of aldehyde dehydrogenases using activity- and affinity-based protein profiling techniques. Applications of the first-in-class retinal-based probe, **LEI-945**, include, but are not limited to, the profiling of ALDH activities in cancer in and clarifying vitamin A metabolism in the small intestines. In addition to this tailored retinal probe, the synthesis and use of clickable retinoids are discussed and a broad-spectrum probe for the ALDH family is developed. Together these chemical tools provide researchers with a comprehensive toolkit to study ALDH enzymes. The results obtained using these chemical tools showcase the application of substrate-based probes in interrogating pathologically relevant enzyme activities. They also highlight the general power of chemical proteomics in driving the discovery of new biological insights and its utility to guide drug discovery efforts.

Acknowledgements

Lukas Wijaya and Sylvia Le Dévédec are kindly acknowledged for performing and analyzing the live cell imaging, and Freek Ariese for recording the Raman spectra.

Experimental procedures

Biological methods

Cell culture. The breast cancer cell lines BT-20, HCC38, MCF7, MDA-MB-231, MDA-MB-468, SK-BR-3 and SK-BR-7 were grown in RPMI-1640 with stable glutamine and phenol red with 10% Fetal Calf serum, penicillin and streptomycin at 37 °C and 5% CO_2. Medium was refreshed every 2-3 days and cells were passaged twice a week. Cell lines were purchased from ATCC and were regularly tested for mycoplasma contamination. Cultures were discarded after 2-3 months of use.

Cell viability and proliferation. Breast cancer cells were grown to 80% confluency in 10 cm plates. Cells were then seeded in a 96-wells plate depending on their rate of growth (BT-20: 12k/well; MDA-MB-468 & SK-BR-3: 10k/well; SK-BR-7 & HCC38: 8k/well; MDA-MB-231: 4k/well). For the SRB proliferation assay cells were also seeded on an extra plate to be able to determine the starting point protein content. Cells were allowed to adhere overnight and were then treated with vehicle (0.1% DMSO) or inhibitor NCT-505 (30 µM, 0.1% DMSO) in 100 µL RPMI medium. Cells were then incubated for 72 hours. For the MTT viability assay another 100 µL of medium containing MTT (1 mg/mL) was added and the cells were incubated for another 4 hours. The medium was then removed and the formazan crystals were dissolved in 100 µL DMSO during 1 hour in the stove. The absorbance was then measured in a CLARIOstar Plus plate reader at 570 nm. For the SRB assay cells were fixated by incubation with 30 µL 50% TCA for 1 hour at 4 °C. The plates were washed 5 times with water and dried. 60 µL 0.4% SRB was added and incubated for 30 minutes at room temperature. The plates were then washed another four times with acetic acid (0.1%) and dried. The SRB was dissolved by adding 150 µL Tris (10 mM) and incubating for 30 minutes at room temperature. Absorbance was then measured at 540 nm on a CLARIOstar Plus plate reader. Graphpad Prism® 7 (Graphpad Software Inc.) was used to plot data and calculation of mean values and standard deviation.

Combination of NCT-505 and Fer-1. MDA-MB-468 cells were seeded in 96-wells plates at 10k/well. Cells were allowed to adhere overnight and were then treated with vehicle (0.1% DMSO), NCT-505 (30 µM, 0.1% DMSO), Fer-1 (10 µM, 0.1% DMSO, Sigma-Aldrich) or a combination of NCT-505 (30 µM) and RSL3 (10 µM). Cells were then incubated for 72 hours and a MTT assay was performed as described above. Graphpad Prism® 7 (Graphpad Software Inc.) was used to plot data and calculation of mean values and standard deviation.

Live cell imaging

Exposure and live cell imaging. Cells were seeded in Greiner black µ-CLEAR 96 well plates at 10k/well. Prior to the NCT-505 exposure, the cells were incubated with 100 ng/ml live Hoechst 33342 in complete RPMI for 2 hours. Thereafter, the medium was refreshed with complete medium. For cell death experiment, 0.2 µM propidium iodide (PI) and Annexin-V-Alexa633 (AnV) were added to the complete medium. For the live mitochondrial membrane potential imaging, the cells were incubated with rhodamine123 dye (0.5 µM; Sigma Aldrich) in combination with live Hoechst 33342 for 2 hours, thereafter we refreshed with complete medium containing rhodamine123 only (0.075 µM) for time-lapse imaging. Then complete medium containing vehicle or NCT-505 (30 µM final concentration) was added and the plates were directly imaged onto the microscope stage for live cell imaging.

For the cell death experiment and mitochondrial membrane potential imaging, the plates were imaged at 0, 14, 24, 40, and 72 hours after the compound exposure. The cell cycle was imaged every hour after the exposure. The imaging was performed using a Nikon TiE2000 confocal laser microscope (lasers : 647 nm, 540 nm, 488 nm, and 408 nm), equipped with automated stage and perfect focus system. During the imaging, the plates were maintained in humidified atmosphere at 37 °C and 5% CO_2. The experiment was conducted with 3 biological replicates with 4-5 technical replicates.

Image analysis. The quantitative image analysis was performed with ImageJ version 1.52p, CellProfiler version 2.2.0 and Ilastik 1.3.2. Firstly, the nuclei per image were segmented using the watershed masked algorithm on ImageJ. For images obtained from the cell death and mitochondrial membrane potential experiment, the nuclear segmentation was performed with Ilastik 1.3.2. The images were processed with an in house developed CellProfiler module[49,50]. For the cell death and mitochondrial membrane potential experiment , the nuclear Hoechst 33342 intensity levels, rhodamine 123 integrated intensity, PI area, and Annexin V area were measured at the single cell level. The results were stored as HDF5 files. Data analysis, quality control, and graphics were performed using the in house developed R package h5CellProfiler (manuscript in preparation).

References

1. Koppaka, V. *et al.* Aldehyde Dehydrogenase Inhibitors: a Comprehensive Review of the Pharmacology, Mechanism of Action, Substrate Specificity, and Clinical Application. *Pharmacol. Rev.* **64**, 520–539 (2012).
2. Duester, G., Mic, F. A. & Molotkov, A. Cytosolic retinoid dehydrogenases govern ubiquitous metabolism of retinol to retinaldehyde followed by tissue-specific metabolism to retinoic acid. in *Chemico-Biological Interactions* **143**–**144**, 201–210 (Elsevier, 2003).
3. Vasiliou, V., Pappa, A. & Petersen, D. R. Role of aldehyde dehydrogenases in endogenous and xenobiotic metabolism. *Chem. Biol. Interact.* **129**, 1–19 (2000).
4. Kurys, G., Ambroziak, W. & Pietruszkos, R. Human Aldehyde Dehydrogenase. *J. Biol. Chem.* **264**, 4715–4721 (1989).
5. Kutzbach, C. & Stokstad, E. L. R. Mammalian methylenetetrahydrofolate reductase Partial purification, properties, and inhibition by S-adenosylmethionine. *BBA - Enzymol.* **250**, 459–477 (1971).
6. Chern, M. K. & Pietruszko, R. Human aldehyde dehydrogenase E3 isozyme is a betaine aldehyde dehydrogenase. *Biochem. Biophys. Res. Commun.* **213**, 561–568 (1995).
7. Jackson, B. *et al.* Update on the aldehyde dehydrogenase gene (ALDH) superfamily. *Hum. Genomics* **5**, 283–303 (2011).
8. Zile, M. H. Vitamin A and Embryonic Development: An Overview. *J. Nutr.* **128**, 455–458 (1998).
9. Wiseman, E. M., Bar-El Dadon, S. & Reifen, R. The vicious cycle of vitamin a deficiency: A review. *Crit. Rev. Food Sci. Nutr.* **57**, 3703–3714 (2017).
10. Mora, J. R., Iwata, M. & Andrian, U. H. Von. Vitamin effects on the immune system. *Nat. Rev. Immunol.* **8**, 685–698 (2008).
11. Blomhoff, H. K. *et al.* Vitamin A is a key regulator for cell growth, cytokine production, and differentiation in normal B cells. *J. Biol. Chem.* **267**, 23988–23992 (1992).
12. Carlberg, C. Lipid soluble vitamins in gene regulation. *BioFactors* **10**, 91–97 (1999).
13. Balmer, J. E. & Blomhoff, R. Gene expression regulation by retinoic acid. *J. Lipid Res.* **43**, 1773–808 (2002).
14. D'Ambrosio, D. N., Clugston, R. D. & Blaner, W. S. Vitamin A metabolism: An update. *Nutrients* **3**, 63–103 (2011).
15. Wang, J. *et al.* Phosphorylation-dependent regulation of ALDH1A1 by Aurora kinase A: Insights on their synergistic relationship in pancreatic cancer. *BMC Biol.* **15**, 1–22 (2017).
16. Zhao, D. *et al.* NOTCH-induced aldehyde dehydrogenase 1A1 deacetylation promotes breast cancer stem cells. *J. Clin. Invest.* **124**, 5453–5465 (2014).
17. Koenders, S. T. A., Gagestein, B. & van der Stelt, M. Opportunities for lipid-based probes in the field of immunology. in *Current Topics in Microbiology and Immunology* **420**, 283–319 (Springer, Cham, 2018).
18. Serwa, R. & Tate, E. W. Activity-based profiling for drug discovery. *Chemistry and Biology* **18**, 407–409 (2011).
19. Cravatt, B. F., Wright, A. T. & Kozarich, J. W. Activity-Based Protein Profiling: From Enzyme Chemistry to Proteomic Chemistry. *Annu. Rev. Biochem.* **77**, 383–414 (2008).
20. Koenders, S. T. A. *et al.* Development of a Retinal-Based Probe for the Profiling of Retinaldehyde Dehydrogenases in Cancer Cells. *ACS Cent. Sci.* **5**, 1965–1974 (2019).
21. Croker, A. K. & Allan, A. L. Inhibition of aldehyde dehydrogenase (ALDH) activity reduces chemotherapy and radiation resistance of stem-like ALDH hiCD44 + human breast cancer cells. *Breast Cancer Res. Treat.* **133**, 75–87 (2012).
22. Qiu, Y. *et al.* The expression of aldehyde dehydrogenase family in breast cancer. *J. Breast Cancer* **17**, 54–60 (2014).
23. Marcato, P. *et al.* Aldehyde Dehydrogenase Activity of Breast Cancer Stem Cells Is Primarily Due To Isoform ALDH1A3 and Its Expression Is Predictive of Metastasis. *Stem Cells* **29**, 32–45 (2011).
24. Sládek, N. E., Kollander, R., Sreerama, L. & Kiang, D. T. Cellular levels of aldehyde dehydrogenases (ALDH1A1 and ALDH3A1) as predictors of therapeutic responses to cyclophosphamide-based chemotherapy of breast cancer: A retrospective study. *Cancer Chemother. Pharmacol.* **49**, 309–321 (2002).
25. Tomita, H., Tanaka, K., Tanaka, T. & Hara, A. Aldehyde dehydrogenase 1A1 in stem cells and cancer. *Oncotarget* **7**, 11018–32 (2016).
26. De Beca, F. F. *et al.* Cancer stem cells markers CD44, CD24 and ALDH1 in breast cancer special histological types. *J. Clin. Pathol.* **66**, 187–191 (2013).
27. Yang, S. M. *et al.* Discovery of Orally Bioavailable, Quinoline-Based Aldehyde Dehydrogenase 1A1 (ALDH1A1) Inhibitors with Potent Cellular Activity. *J. Med. Chem.* **61**, 4883–4903 (2018).
28. Reynolds, D. S. *et al.* Breast Cancer Spheroids Reveal a Differential Cancer Stem Cell Response to Chemotherapeutic Treatment.

Sci. Rep. **7**, 1–12 (2017).

29. Fujiwara, D., Kato, K., Nohara, S., Iwanuma, Y. & Kajiyama, Y. The usefulness of three-dimensional cell culture in induction of cancer stem cells from esophageal squamous cell carcinoma cell lines. *Biochem. Biophys. Res. Commun.* **434**, 773–778 (2013).
30. Marcato, P., Dean, C. A., Giacomantonio, C. A. & Lee, P. W. K. Aldehyde dehydrogenase its role as a cancer stem cell marker comes down to the specific isoform. *Cell Cycle* **10**, 1378–1384 (2011).
31. Dixon, S. J. *et al.* Ferroptosis: An iron-dependent form of nonapoptotic cell death. *Cell* **149**, 1060–1072 (2012).
32. Yang, W. S. *et al.* Regulation of ferroptotic cancer cell death by GPX4. *Cell* **156**, 317–331 (2014).
33. Brash, A. R. Lipoxygenases: Occurrence, functions, catalysis, and acquisition of substrate. *Journal of Biological Chemistry* **274**, 23679–23682 (1999).
34. Viswanathan, V. S. *et al.* Dependency of a therapy-resistant state of cancer cells on a lipid peroxidase pathway. *Nature* **547**, 453–457 (2017).
35. de Jesus, B. B. & Blasco, M. A. Assessing cell and organ senescence biomarkers. *Circ. Res.* **111**, 97–109 (2012).
36. Martinez Molina, D. & Nordlund, P. The Cellular Thermal Shift Assay: A Novel Biophysical Assay for In Situ Drug Target Engagement and Mechanistic Biomarker Studies. *Annu. Rev. Pharmacol. Toxicol.* **56**, 141–161 (2016).
37. Dziekan, J. M. *et al.* Identifying purine nucleoside phosphorylase as the target of quinine using cellular thermal shift assay. *Sci. Transl. Med.* **11**, (2019).
38. Svensson, M. *et al.* CCL25 mediates the localization of recently activated CD8αβ+lymphocytes to the small-intestinal mucosa. *J. Clin. Invest.* **110**, 1113–1121 (2002).
39. Hamann, A., Andrew, D. P., Jablonski-Westrich, D., Holzmann, B. & Butcher, E. C. Role of alpha 4-integrins in lymphocyte homing to mucosal tissues in vivo. *J. Immunol.* **152**, 3282–93 (1994).
40. Jaensson-Gyllenbäck, E. *et al.* Bile retinoids imprint intestinal CD103+ dendritic cells with the ability to generate gut-tropic T cells. *Mucosal Immunol.* **4**, 438–447 (2011).
41. Dunagin, P. E., Zachman, R. D. & Oslo, J. A. The identification of metabolites of retinal and retinoic acid in rat bile. *BBA* **124**, 71–85 (1966).
42. Whidbey, C. *et al.* A Probe-Enabled Approach for the Selective Isolation and Characterization of Functionally Active Subpopulations in the Gut Microbiome. *J. Am. Chem. Soc.* **141**, 42–47 (2019).
43. Jamieson, L. E. *et al.* Tracking intracellular uptake and localisation of alkyne tagged fatty acids using Raman spectroscopy. *Spectrochim. Acta - Part A Mol. Biomol. Spectrosc.* **197**, 30–36 (2018).
44. Yamakoshi, H. *et al.* Alkyne-tag Raman imaging for visualization of mobile small molecules in live cells. *J. Am. Chem. Soc.* **134**, 20681–20689 (2012).
45. Failloux, N., Bonnet, I., Baron, M. H. & Perrier, E. Quantitative Analysis of Vitamin A Degradation by Raman Spectroscopy. *Appl. Spectrosc.* **57**, 1117–1122 (2003).
46. Khanna, M. *et al.* Discovery of a novel class of covalent inhibitor for aldehyde dehydrogenases. *J. Biol. Chem.* **286**, 43486–43494 (2011).
47. Parajuli, B., Fishel, M. L. & Hurley, T. D. Selective ALDH3A1 inhibition by benzimidazole analogues increase mafosfamide sensitivity in cancer cells. *J. Med. Chem.* **57**, 449–461 (2014).
48. Moreb, J. S., Muhoczy, D., Ostmark, B. & Zucali, J. R. RNAi-mediated knockdown of aldehyde dehydrogenase class-1A1 and class-3A1 is specific and reveals that each contributes equally to the resistance against 4-hydroperoxycyclophosphamide. *Cancer Chemother. Pharmacol.* **59**, 127–136 (2007).
49. Wink, S., Hiemstra, S., Herpers, B. & van de Water, B. High-content imaging-based BAC-GFP toxicity pathway reporters to assess chemical adversity liabilities. *Arch. Toxicol.* **91**, 1367–1383 (2017).
50. Yan, K. & Verbeek, F. J. Segmentation for high-throughput image analysis: Watershed masked clustering. in *Lecture Notes in Computer Science (including subseries Lecture Notes in Artificial Intelligence and Lecture Notes in Bioinformatics)* **7610**, 25–41 (Springer, Berlin, Heidelberg, 2012).